Journal of Biomechanics 83 (2019) 65–75

Contents lists available at ScienceDirect

Journal of Biomechanics

journal homepage: www.elsevier.com/locate/jbiomech
www.JBiomech.com

Interrelationship of cartilage composition and chondrocyte mechanics after a partial meniscectomy in the rabbit knee joint – Experimental and numerical analysis

A.P. Ronkainen [a,*], P. Tanska [a], J.M. Fick [a], W. Herzog [b], R.K. Korhonen [a]

[a] Department of Applied Physics, University of Eastern Finland, Kuopio FI-70211, Finland
[b] Human Performance Laboratory, Faculty of Kinesiology, University of Calgary, Calgary, Alberta, Canada

ARTICLE INFO

Article history:
Accepted 14 November 2018

Keywords:
Articular cartilage
Chondrocyte
Extracellular matrix
Finite element modeling
Pericellular matrix

ABSTRACT

Site-specific and depth-dependent properties of cartilage were implemented within a finite element (FE) model to determine if compositional or structural changes in the tissue could explain site-specific alterations of chondrocyte deformations due to cartilage loading in rabbit knee joints 3 days after a partial meniscectomy (PM). Depth-dependent proteoglycan (PG) content, collagen content and collagen orientation in the cartilage extracellular matrix (ECM), and PG content in the pericellular matrix (PCM) were assessed with microscopic and spectroscopic methods. Patellar, femoral groove and samples from both the lateral and medial compartments of the femoral condyle and tibial plateau were extracted from healthy controls and from the partial meniscectomy group. For both groups and each knee joint site, axisymmetric FE models with measured properties were generated. Experimental cartilage loading was applied in the simulations and chondrocyte volumes were compared to the experimental values. ECM and PCM PG loss occurred within the superficial cartilage layer in the PM group at all locations, except in the lateral tibial plateau. Collagen content and orientation were not significantly altered due to the PM. The FE simulations predicted similar chondrocyte volume changes and group differences as obtained experimentally. Loss of PCM fixed charge density (FCD) decreased cell volume loss, as observed in the medial femur and medial tibia, whereas loss of ECM FCD increased cell volume loss, as seen in the patella, femoral groove and lateral femur. The model outcome, cell volume change, was also sensitive to applied tissue geometry, collagen fibril orientation and loading conditions.

1. Introduction

Late stages of osteoarthritis (OA) are well documented (e.g., erosion of cartilage, damage to subchondral bone and total loss of joint function), but what occurs in the early stages and during the onset of the disease is of current interest and pivotal in disease prevention and early intervention (Sharma, 2016). Because OA onset is faster in animals than in humans and sample populations are more controlled, animal models are frequently used to study OA. A partial meniscectomy (PM) creates abnormal load magnitudes and distributions within the knee joint (Arunakul et al., 2013; Mansour et al., 1998), ultimately leading to post-traumatic OA in rabbits (Colombo et al., 1983; Sokoloff, 1990). PMs are also associated with post-operative knee OA in humans, and the extent of meniscal resection is an important predictor for disease development (Papalia et al., 2011).

Cartilage damage has been observed a mere 3 days following a PM in the lateral knee joint compartment of rabbits (Colombo et al., 1983). At this time point, superficial proteoglycan (PG) depletion, followed by a formation of cartilage lesions at 1 to 2 weeks post-surgery was reported. The equilibrium modulus of cartilage, coupled with the uronic acid content (PG content), was decreased in tibial cartilages 1 week after a total medial meniscectomy (Hoch et al., 1983) and collagen type II breakdown was observed at the 2 week time-point (Lindhorst et al., 2005). Altogether, these studies imply that cartilage PG content decreases within days, and the collagen network degrades within weeks of surgical intervention in the rabbit knee joint.

At microscopic-scale, alterations in the cartilage structure take place concurrently with altered deformation behavior of chondrocytes due to tissue loading (Han et al., 2017), and deformation of chondrocytes affects the cell synthesis, proliferation, apoptosis

* Corresponding author at: Department of Applied Physics, University of Eastern Finland, Yliopistonranta 1F, POB 1627, Kuopio FI-70211, Finland.
E-mail address: ari.p.ronkainen@uef.fi (A.P. Ronkainen).

https://doi.org/10.1016/j.jbiomech.2018.11.024
0021-9290/

and differentiation (Elder et al., 2001). It is also known that the local mechanical properties of the pericellular matrix (PCM) are affected in early OA progression, which may affect its protective role (Wilusz et al., 2014). However, it is still controversial as to how much the PCM composition is altered in early OA, although an intact PCM appears vital for cell survival (de Vries et al., 2014). As complex alterations in tissue composition and structure occur during OA, it can be difficult to identify how a single alteration (e.g., PG depletion or collagen network damage) affects tissue and cell mechanics, and mechano-transduction. To address this challenge, multi-scale computational finite element (FE) modeling has proven powerful when studying cartilage and cell mechanics (Halloran et al., 2012). However, more knowledge about the validity of cell-level models is warranted, as this information is scarce. This specifically includes FE models that include experimentally measured compositional and structural parameters for articular cartilage.

In a previous study (Fick et al., 2016), we investigated chondrocyte volume changes under indentation loading at six locations in the rabbit knee, and tested if lateral PM affects chondrocyte volume changes 3 days after surgery. In situ chondrocytes lost volume when tissues were subjected to experimental indentation loading, and these cell volume losses were significantly altered 3 days after the surgery. Simultaneously, superficial PG content had decreased throughout the joint. However, the cell volume losses were decreased in the medial femoral and tibial cartilages, whereas cell volume losses were increased in the patellar, femoral groove and lateral femoral cartilages 3 days after PM surgery. Hence PG depletion in the cartilage ECM could not directly explain the altered mechanical behavior of chondrocytes at different joint locations. However, previous experimental (Ronkainen et al., 2016) and theoretical studies (Tanska et al., 2013) have suggested that PCM PG content and articular cartilage collagen content are associated with cell responses, and thus, it would be important to investigate if alterations in the collagen network and PCM PG content due to the PM surgery occurred within 3 days of PM surgery.

As the reasons for the altered cell volume changes due to the PM surgery remained elusive in Fick et al. (2016), we aimed to study if these results could be explained by differences in the articular cartilage ECM and PCM properties, i.e., tissue depth-dependent PG content, collagen content, collagen fibril orientation, and pericellular PG content. Based on previous studies (Ronkainen et al., 2016; Tanska et al., 2013), our primary hypotheses were that the observed loss of PGs in the ECM could explain the increased cell volume losses 3 days after PM, whereas the loss of PGs in the PCM could explain the decreased cell volume losses after PM. In order to test our hypotheses, we used a multi-scale FE model of articular cartilage for simulating how changes in the experimentally measured composition and structure of articular cartilage due to PM would affect the cell volume changes.

2. Methods

2.1. Samples, sample processing and cell deformations

Samples collected in previous studies were used (Fick et al., 2016, 2015). These samples were obtained from six locations of the knee joint (Fig. 1) of New Zealand White rabbits (n = 10 knees/group) from partially meniscectomized rabbit knees (PM group), their contralateral limbs (C-L group) and from non-operated rabbit knees (CNTRL group). Cell deformation experiments were previously performed (Fig. 2A and B) within 48 h of sample collection. Samples were then fixed and stored in formalin and sections for histology were prepared (Fick et al., 2015; Ronkainen et al., 2016). For more details on these previously performed steps, see supplementary materials.

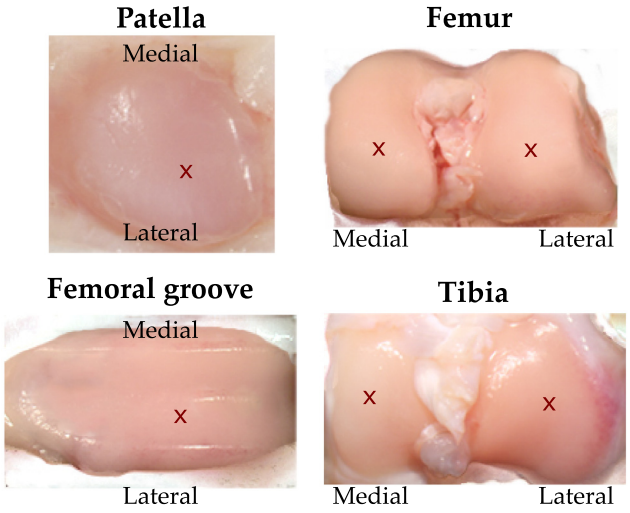

Fig. 1. The six studied rabbit knee joint locations, with the "x" marking the location of indentation testing.

2.2. Cartilage composition and structure

Cartilage composition and structure was analyzed previously for the CNTRL group samples (Ronkainen et al. 2016). This included cartilage ECM-level data of collagen fibril orientation, proteoglycan content and collagen content assessed by polarized light microscopy (PLM), digital densitometry (DD) and Fourier transform infrared imaging (FTIR), respectively. In addition, the PCM-level PG content was analyzed using the DD at higher magnification (Ronkainen et al. 2016).

In the current study, we reanalyzed previously measured (Fick et al., 2016) ECM-level PG content and collagen fibril orientation data in a depth-dependent manner for the C-L and PM groups, in order to implement our site-specific FE models (Fig. 2C and D) with realistic and site-specific tissue composition and structural information (Fig. 2E). In addition, we measured the cartilage collagen content and the PCM-level PG content for the C-L and PM groups using FTIR and DD, respectively. For FTIR, we prepared new sections from the stored osteochondral blocks, whereas for the PCM-level DD, the old sections could be used (Fick et al., 2016). Detailed descriptions of PLM, DD and FTIR are included in the supplementary materials, as these methods have been extensively used and described previously (Camacho et al., 2001; Kiviranta et al., 1985; Potter et al., 2001; Rieppo et al., 2008; Ronkainen et al., 2016).

3. Finite element model

3.1. Model generation

In order to clarify the effects of the aforementioned cartilage composition and structure on cell volume changes (see our hypotheses), axisymmetric, multi-scale FE models (Fig. 2C) with experimentally measured composition and structure were constructed for the CNTRL and PM groups (cell deformations and tissue properties of the C-L group were similar to those of the CNTRL group (Fick et al., 2016), thus models for that group were not needed). A separate model was constructed for each knee joint location (Fig. 1; patella, femoral groove, lateral femur, medial femur, lateral tibia, medial tibia) for both groups (CNTRL and PM,

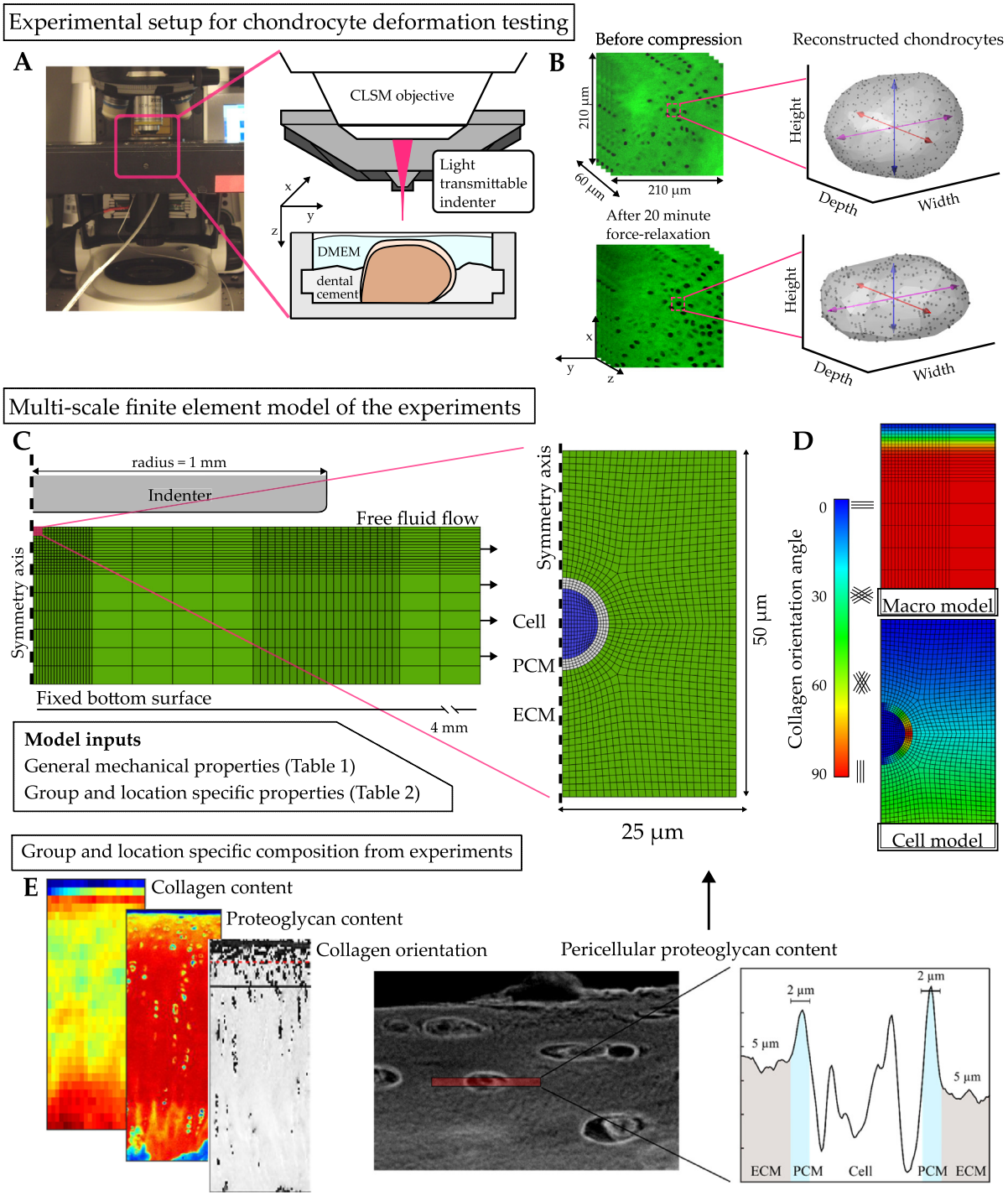

Fig. 2. (A) Confocal laser scanning microscope equipped with a light-transmittable indenter (d = 2 mm) was used to image chondrocytes before and after indentation (Fick et al., 2016, 2015). Cartilage-on-bone samples were fixed in a sample holder using dental cement and immersed in Dulbecco's Modified Eagle Medium (DMEM) during testing. Indentation was performed at constant velocity (10 µm/s) until 2 MPa nominal pressure was reached. (B) To calculate chondrocyte volume changes, 10 chondrocytes from before and after loading image stacks were identified, cropped and had their volume reconstructed. (C) Axisymmetric multi-scale FE model was generated to replicate the experiments. The cell model was located in the first 50 µm of cartilage depth and next to the symmetry axis as shown. (D) Example of collagen orientation in the FE model. (E) Knee joint location and group specific cartilage composition was implemented (details in supplementary materials) according to measured microscopic data.

n = 6 models/group) (Fig. 2C). Each of the twelve FE models was implemented with the average composition and structure of the given knee joint location, as determined through the microspectroscopic and microscopic methods for collagen content, PG content and collagen fibril orientation (n = 10 samples per location) (Fig. 2E). Each multi-scale FE model consisted of a macro-scale cartilage model (n = 6/group) and a micro-scale cell model (n = 6/group). The ECM and PCM were modelled using fibril-reinforced, poroelastic, swelling (FRPES) material properties (Table 1) (Julkunen et al., 2013; Tanska et al., 2013; Wilson, 2005; Wilson et al., 2006, 2005) and the same ECM behaviour was implemented on both the macro and micro-scale models for consistency between the ECM and PCM. As this material model has been characterized extensively in these previous studies, the

Table 1
General mechanical properties for the ECM, PCM and chondrocyte in the FE models. One order of magnitude difference between the PCM and ECM properties was implemented (Guilak et al., 2005; Korhonen et al., 2008). Cell properties were assumed from earlier studies (Florea et al., 2016; Guilak et al., 2002; Korhonen et al., 2015). Normalized depth z (0 = cartilage surface, 1 = cartilage-bone interface) was used to implement decreasing fluid volume fraction in the ECM (Wilson et al., 2005). Parameters based on PLM, DD and FTIR data were different for each model (for examples, see supplemental Figs. 1 and 2) and E_f, E_m and k_0 were different between joint locations (Table 2).

Parameter (units)	ECM	PCM	Chondrocyte
E_f(MPa)	[3.0–7.0]*	$10\% \cdot E_f^{ECM}$	–
E_m(MPa)	[0.7–1.3]*	$10\% \cdot E_m^{ECM}$	$3.3\% \cdot E_m^{ECM}$
k_0(10^{-15} m^4 N^{-1} s^{-1})	[1.3–3.5]*	$10\% \cdot k_0^{ECM}$	0.79
υ_m	0.42	0.3	0.3
M	8.1	–	–
n_f	0.85–0.15z	0.85	0.6
θ_{col}(°)	PLM data (Sup. Fig. 2)	Tangential to cell surface	–
ρ_z	FTIR data (Sup. Fig. 3)	ρ_z^{ECM}	–
c_f(mEq ml^{-1})	DD data (Fig. 2)	Cell-level DD data (Fig. 6)	$90\% \cdot c_f^{ECM}$

E_f = fibril network modulus, E_m = non-fibrillar matrix modulus, k_0 = initial permeability, θ_{col} = primary fibril orientation, c_f = fixed charge density, ρ_z = relative fibril volume density, υ_m = Poisson's ratio of the non-fibrillar matrix, M = permeability strain-dependency factor, n_f = fluid volume fraction.
* Parameter is knee joint location-specific (see Table 2) [minimum – maximum] range is given.

details are included in the supplementary materials. Model geometries (Fig. 2C) were based on the experimental microscopy data, for details, see supplementary materials.

3.2. Implementation of measured composition

The collagen orientation was implemented into the FE models (Fig. 2D and 2E) based on the experimentally measured PLM data of the samples (Fick et al., 2016; Supplemental Fig. 4). Implementation was performed as described previously (Julkunen et al., 2007; Tanska et al., 2013; Wilson et al., 2004) with 2 variables: superficial zone thickness (d_{vec}) and bending radius of the collagen fibrils in the middle zone (r_{vec}), see supplementary materials for an example. The collagen content was implemented with a relative fibril volume density (ρ_z), which was estimated from the FTIR data (Supplemental Fig. 5), as described previously (Mäkelä and Korhonen, 2016) by fitting a line to the normalized collagen content (Supplemental Fig. 2).

The FCD in the swelling equations (see supplemental equations S7 and S8) was acquired from the DD data by converting experimental optical density (OD) profiles into FCD according to Király et al. (1996)

$$\mathrm{FCD} = \frac{\mathrm{OD} + 1.105}{15.153}\,\mathrm{mEq/ml}. \quad (1)$$

The ECM FCD (c_F^{ECM}) at different depths in the model was calculated by fitting a 12th order polynomial to the FCD profiles (Supplemental Fig. 2). The FCD in the PCM (c_F^{PCM}) was calculated from the surrounding ECM FCD as

$$c_F^{PCM} = \alpha_{PCM} \cdot c_F^{ECM}, \quad (2)$$

where the multiplier α_{PCM} was calculated from the normalized cell-level DD data as the average value from the PCM region (region marked in Fig. 6, for values see Table 2).

3.3. Mechanical properties

After implementing the measured composition and structure in the models, the material properties of the ECM (collagen network modulus, E_f, non-fibrillar matrix modulus, E_m, and initial permeability, k_0; Table 2) were optimized. The rest of the material parameters of the ECM were obtained from the literature and were identical in all models (Table 1). Optimization was carried out by simulating the experimental indentation protocol and adjusting these values until the difference between the experimental and simulated peak and equilibrium contact pressures was less than 2% (Table 2). The same optimized parameter values were used for both the CNTRL and PM group samples (Table 2), as the PM surgery did not alter the force-response of the tissue at any knee joint location (peak and equilibrium stresses, strains and moduli) (Fick et al., 2016). Chondrocyte and PCM properties were taken from the literature (Table 1) except for the FCD of the PCM, which was implemented based on the experimental data obtained in the current study (Eq. (2) and Table 2).

3.4. Finite element analysis of cell deformation experiments

The experimental indentation protocol (Fick et al., 2016) was simulated using a multi-scale approach. First, in the macro-scale site models, the indenter was moved into contact with the cartilage surface after free swelling of the tissue. This initial swelling step was included before application of the mechanical loading in order to mimic an experimental reference state where the cartilage is immersed in a physiological environment (0.15 M saline solution) (Julkunen et al., 2009; Korhonen et al., 2008; Wilson et al., 2005). The tissue level response of cartilage indentation was simulated for each site (macro-scale site models), before sim-

Table 2
The FRPES material properties were optimized for each knee joint location. Optimization criteria for E_f, E_m and k_0 were to minimize the absolute errors (<2%) between the experimental and simulated peak and equilibrium pressures in indentation testing. Zonal thicknesses were same in CNTRL and PM groups (Supplemental Fig. 4), whereas the PCM to ECM fixed charge density (Fig. 6) and cartilage thicknesses were experimentally measured for both groups.

Parameter (units)		Patella	Groove	Lateral Femur	Lateral Tibia	Medial Femur	Medial Tibia
Optimized	E_f(MPa)	7.0	4.0	6.0	7.0	4.0	3.5
	E_m(MPa)	0.7	1.3	0.8	1.0	0.8	0.7
	k_0(10^{-15} m^{4}N^{-1}s^{-1})	2.0	1.3	3.5	1.5	2.5	1.5
PLM	d_{vec}	5%	10%	6%	9%	5%	3%
	r_{vec}	9%	15%	18%	25%	15%	9%
CNTRL	α_{PCM}	1.119	1.063	1.012	1.044	1.078	1.089
	h	877 μm	538 μm	472 μm	388 μm	559 μm	803 μm
PM	α_{PCM}	1.231	1.142	1.078	1.077	1.170	1.214
	h	831 μm	534 μm	421 μm	384 μm	589 μm	850 μm

E_f = fibril network modulus, E_m = non-fibrillar matrix modulus, k_0 = initial permeability, d_{vec} = superficial zone thickness, r_{vec} = bending radius of middle zone fibrils, α_{PCM} = PCM to ECM fixed charge density, h = cartilage thickness.

ulating microscopic cell models. Note that cells were excluded from the macro-scale site models.

Then, the displacements and pore pressures of the macro-scale model were obtained (by interpolation) from the nodes closest to the boundary nodes of the micro-scale cell model (Fig. 1C). The time varying fluid pressures and displacements were implemented as boundary conditions for the micro-scale cell model, and they produced the loading for the cell-level simulations. The initial swelling step produced slight changes to the initially round cell shapes (i.e. the cell shapes prior to and after the initial swelling step) in the micro-scale models (Korhonen et al., 2008), because the swelling step is governed by the composition (mainly FCD distribution) and mechanical properties of cartilage (see equations S7 and S8 in the supplemental materials).

The indenter-cartilage contact was assumed frictionless. Subsequent indentation steps were displacement-controlled and performed up to experimentally observed axial strains at a compression rate of 10 μm/s. Indentation was followed by a 1200 s relaxation step, as done in the experiments, which was sufficient time to reach equilibrium in all simulations. In each cell

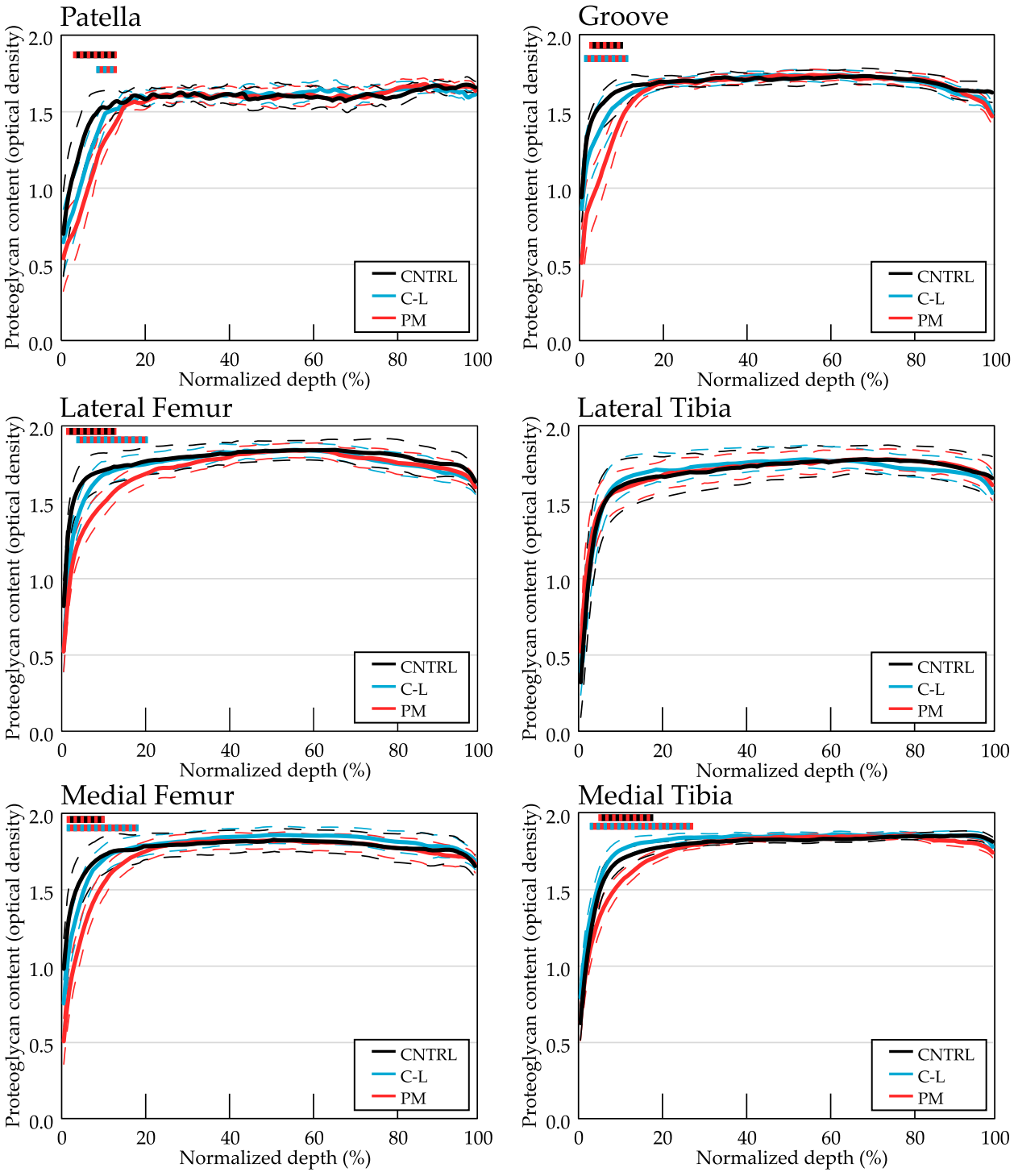

Fig. 3. Proteoglycan content as a function of cartilage depth (normalized to 1–100%) for each studied anatomical location analyzed from previous DD measurements (Fick et al., 2016; Ronkainen et al., 2016) together with Bonferroni adjusted 95% confidence intervals. Point-by-point comparisons between the groups were performed using a linear mixed model. Statistically significant differences ($p < 0.05$) between the groups are indicated with dashed lines above the corresponding depth.

model, volume changes of chondrocytes were calculated as $\frac{V-V_0}{V_0} = \frac{\Delta V}{V_0}$, where V_0 is the initial cell volume after the free swelling step, and V is the cell volume after indentation.

3.5. Parametric analysis

There are uncertainties in the analysed experimental data, especially at the microscopic scale close to the cells. These uncertainties may affect the model results. The specific effect of each property associated with the PM intervention, namely the changes in the FCD of the ECM and PCM, were not individually assessed in the previous analysis. Therefore, in addition to the site-specific models, a parametric analysis was performed to assess how sensitive the model output (i.e., the cell volume change) was to variations in FCD content. In addition, we tested the sensitivity of the cell volume changes to collagen orientation, because this parameter has been linked previously to altered cell deformations (Tanska et al., 2013; Turunen et al., 2013). Since this analysis is generic and invariant to the initial conditions, it was sufficient to use only one model, the CNTRL model of the medial femoral condyle as the baseline for the parametric analysis (i.e., the FCD distribution or collagen orientation was varied while keeping the remaining properties unchanged). Three FCD distributions (range 0.0–0.2 mEq/ml) were considered: varying FCD of the ECM and PCM at the same time (Parametric ECM + PCM), varying FCD of the ECM (Parametric ECM), or varying FCD of the PCM (Parametric PCM). For the parametric analysis of the collagen orientation, the relative thickness of the superficial zone (range 0% - –10%) or the middle zone (range 10% - –20%) was varied.

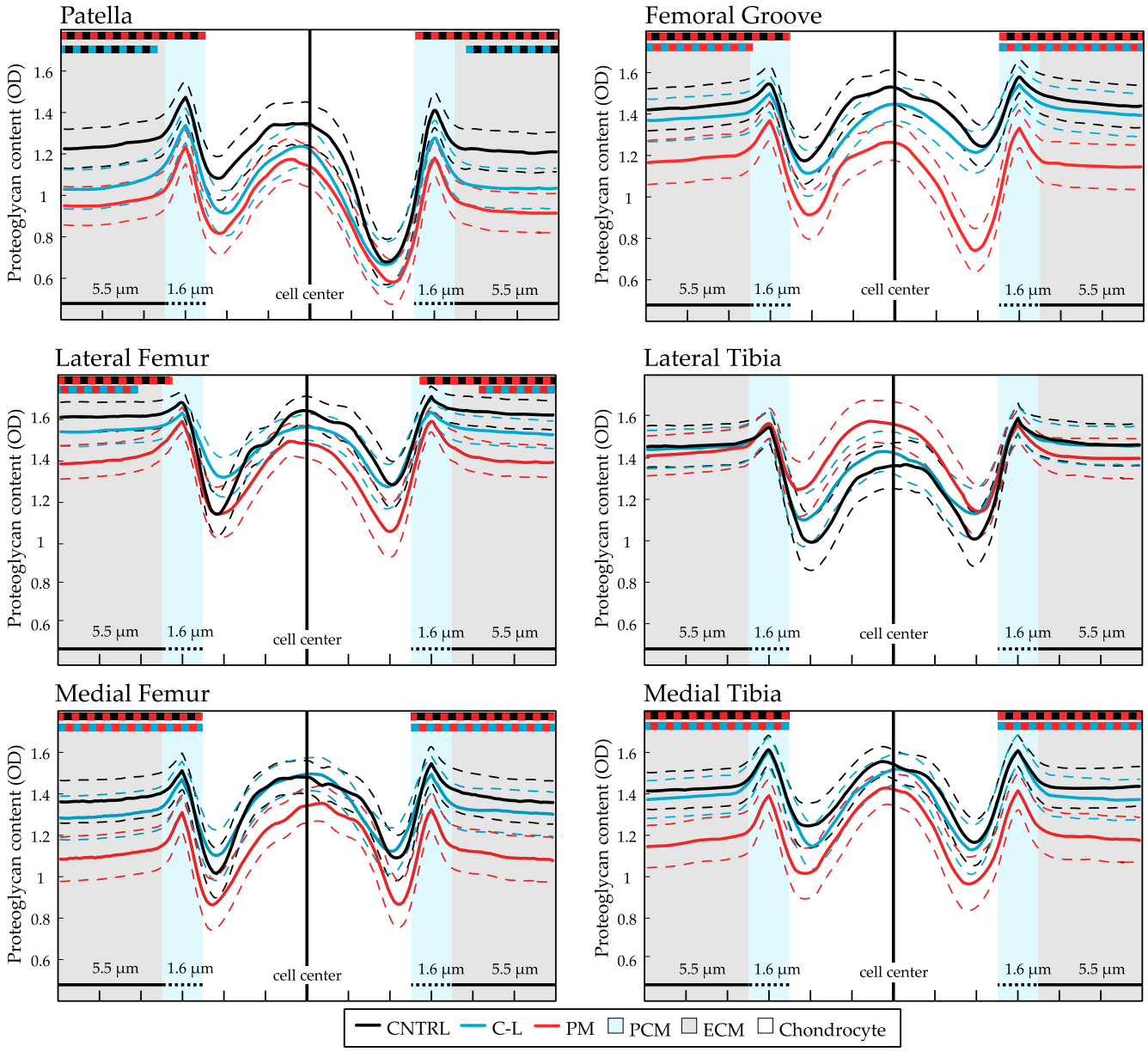

Fig. 4. Cell-level average PG content profiles for each anatomical location with Bonferroni adjusted 95% confidence intervals. Individual profiles were attained by drawing a region of interest through the cell, parallel to its major axis (see supplemental Fig. 3). The resulting profile starts from the ECM at both sides and peaks in the PCM region. The profile values inside the chondrocyte were not included in the analysis. Both sides of the cell were included even though the differences between the two sides are small. Point-by-point comparisons between the groups were performed using linear mixed model. Significant differences ($p < 0.05$) between groups are marked with dashed lines at the corresponding locations.

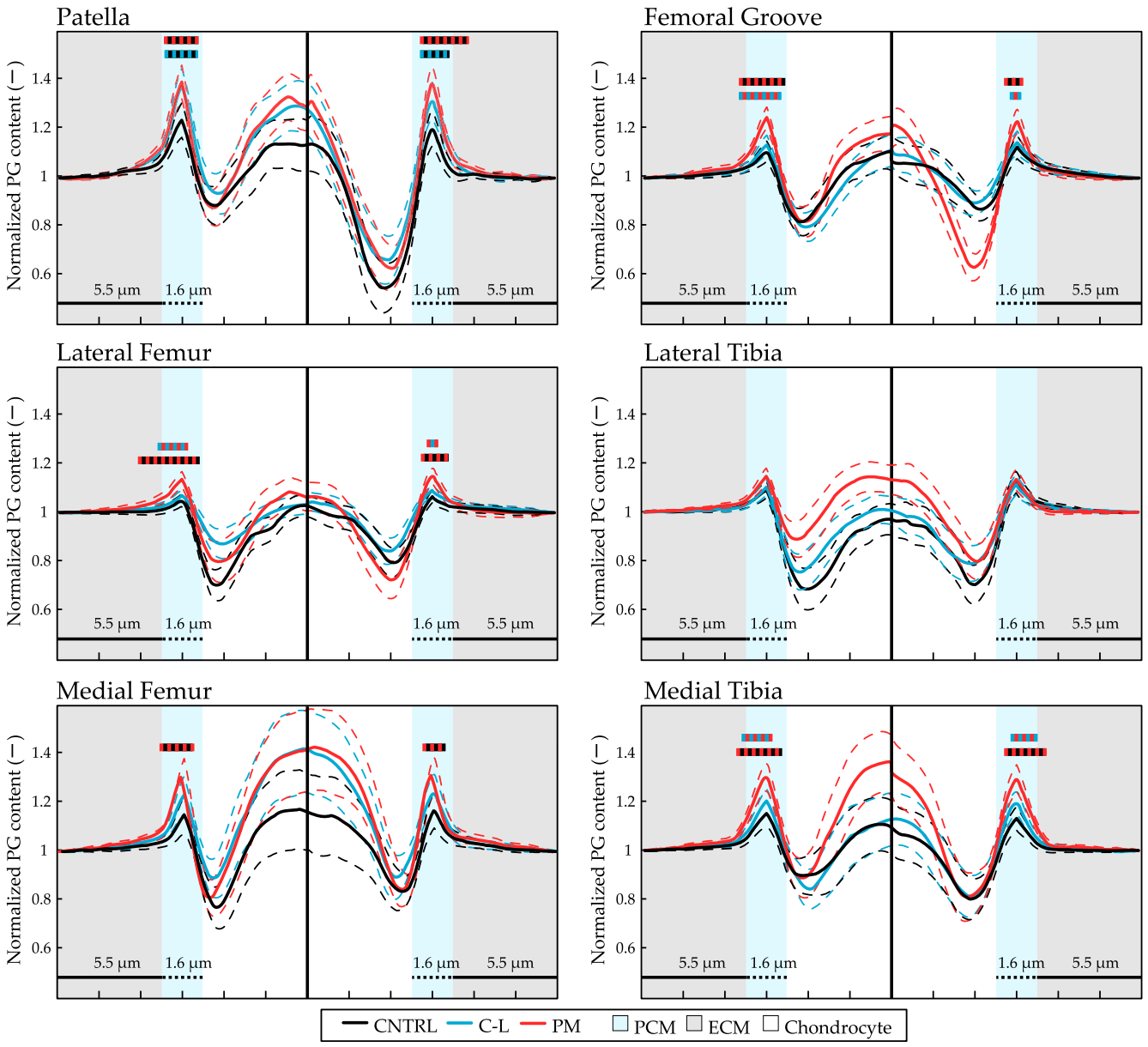

Fig. 5. Normalized cell-level DD profiles. Normalization was performed for each side of the cell separately by dividing the profile with first value in the ECM. Resulting profile was used to approximate how much greater the PCM FCD content on average is (parameter α) by calculating average value from the marked 1.6 μm wide regions (Table 2). Point-by-point comparisons between the groups were performed using linear mixed model. Significant differences ($p < 0.05$) between the groups are marked with dashed lines at the corresponding locations.

3.6. Statistics

Significance of differences in experimentally measured depth-dependent cartilage composition and structure (i.e., PG content, collagen content and collagen orientation) between the groups (CNTRL, C-L, PM) was tested with a linear mixed model (LMM). Bonferroni adjusted 95% confidence intervals were used in testing group differences. For more details on LMM setup, see supplemental materials. All statistical analyses were carried out in SPSS (ver. 21, SPSS Inc., Chicago, IL). All descriptive statistics are given as means ± 95% confidence intervals (CI).

4. Results

4.1. Cartilage ECM and PCM composition

Cartilage collagen content and collagen orientation angle were not significantly different between the CNTRL, PM and C-L groups at any tissue depth (Supplemental Figs. 4 and 5). However, PG loss occurred in the PM group at all locations ($p < 0.05$), except for the lateral tibial plateau, when compared against the CNTRL or C-L group (Fig. 3). This PG loss was restricted to the first 20% of cartilage thickness, with the exception of the medial tibial plateau, where significant PG loss was found up to 30% of the cartilage depth when comparing the PM to the C-L group. Pericellular PG content also decreased in the PM group (Fig. 4), except for the lateral tibial plateau, but this PG loss was not as extensive as that found in the ECM. This result becomes more obvious when the PG content in the pericellular matrix is normalized to the value of the ECM in the immediate vicinity of chondrocytes (Fig. 5).

4.2. FE simulations of chondrocyte deformations

The simulated cell volume changes were similar to those found experimentally (ranging from −5.3% to −19.3% in simulations and

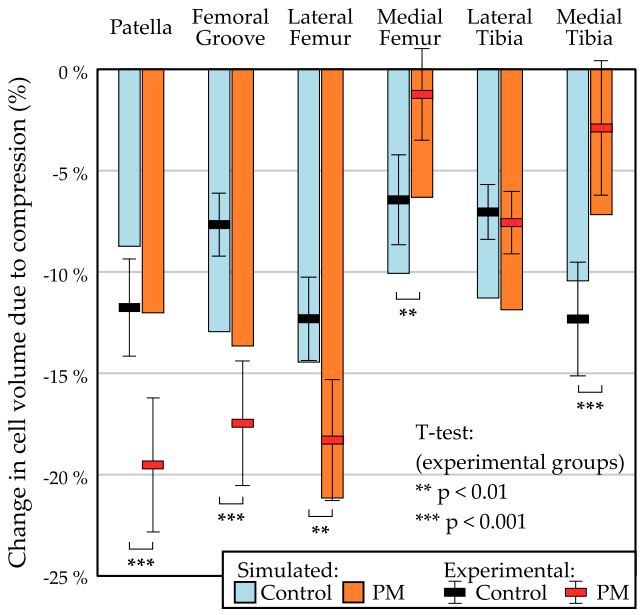

Fig. 6. Experimental and simulated cell volume changes due to indentation loading at each anatomical location. Cell volume changes predicted by FE modeling were similar to those found experimentally and replicated the trend of site-specific group differences. Mean values and 95% confidence intervals are presented for the experimental data, whereas simulated values are shown with the solid bars. Experimental groups are compared to each other with 2-tailed individual samples T-test.

from −1.4% to −19.5% in experiments), and replicated the trend of site-specific group differences (Fig. 6). That is, chondrocytes from the patella, femoral groove and lateral femur of the PM group animals lost more volume during compression than the CNTRL group chondrocytes. In contrast, in the medial femur and tibia, chondrocyte volume loss was reduced in the PM group compared to the CNTRL group samples.

4.3. Parametric analysis

A minor loss of FCD in the ECM from normal, healthy values (around 0.15 mEq/ml) affected the cell volume only little, whereas greater loss of FCD would increase the cell volume loss (Fig. 7). On the other hand, loss of FCD in the PCM from normal, healthy values (around 0.17 mEq/ml) reduced cell volume loss. This latter result was obtained also when FCD was reduced simultaneously both from the ECM and PCM.

Increasing the thickness of the superficial zone from the reference value had little effect on the cell volume response, whereas an increase in the middle zone thickness reduced cell volume loss, and could even cause cell volumes to increase due to the indentation (Fig. 7). Decreasing the thickness of either zone caused a strong increase in cell volume loss.

5. Discussion

5.1. Overview of the experiments and simulations

The depth-dependent composition and structure of rabbit cartilage was analyzed at six rabbit knee joint locations for cartilage harvested 3 days after a partial meniscectomy and compared with previously measured non-operated rabbits. Superficial PGs were lost at this early time point, as shown originally earlier (Fick et al., 2016), without corresponding signs of collagen network disorganization or content changes in the patella, femoral groove, lateral and medial femoral condyles and medial tibial plateau. Pericellular PG content had also decreased at the same knee joint sites in PM group animals. Loss of PGs seems to precede alterations in the collagen network, which implies that this can be used as a target for disease intervention.

The composition-based multi-scale FE models were able to reproduce the magnitude of experimentally measured cell volume changes in each knee joint location of the CNTRL and PM group. The site-specific differences in cell volume changes between the

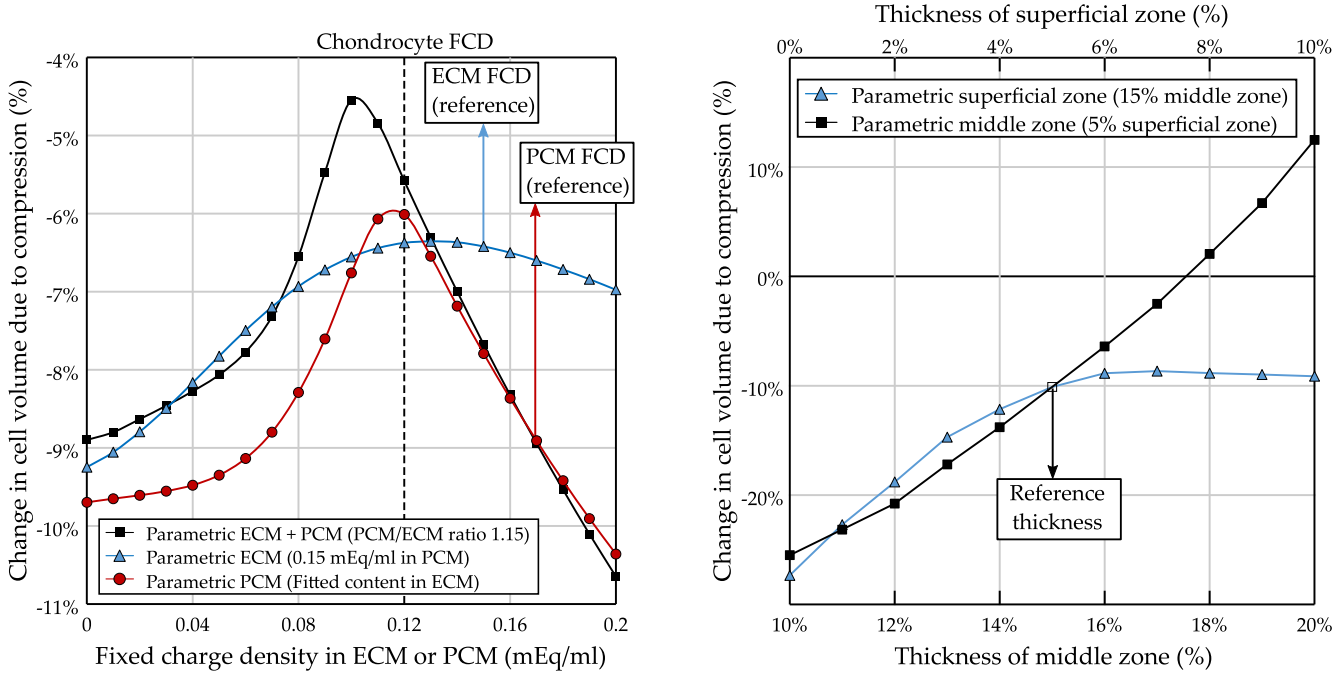

Fig. 7. Parametric analysis on how the fixed charge density (PG content) and the zone thickness (collagen orientation) affect the cell volume change. Each marker corresponds to a one simulation, resulting in a set of 33 unique FCD distributions and 21 different zone thickness variations. Arrows indicate the reference values in the medial femoral condyle tissue of the CNTRL group. The dashed vertical line indicates the implemented chondrocyte fixed charge density. A minimal cell volume loss was observed when the FCD of the PCM was similar to the chondrocyte's FCD. However, alterations in collagen orientation had a greater effect on the cell volume change than alterations of the FCD.

CNTRL and PM groups were also reproduced, although the magnitudes of the cell volume changes were not perfectly predicted. Two mechanisms controlled the cell volume changes in the models: (1) decreased ECM FCD was associated with increased cell volume loss and appeared to be the cause for the cell volume losses observed in the patella, femoral groove and lateral femur after PM. In contrast, (2) decreased PCM FCD was associated with decreased cell volume loss, and appeared to be the cause for the results observed in the medial femur and medial tibial plateau.

The parametric investigation of the FE model showed also that small uncertainties, for example in local collagen orientation, could affect cell volume changes substantially. If we were to implement the full range of values for each model parameter within the uncertainty limits, the exact experimental cell volume changes would likely fall into the range of simulated cell volume changes. However, this was not the aim of the study and was therefore not pursued.

5.2. Experimental outcomes after partial meniscectomy

The PM created significant superficial PG loss at all sites, except for the lateral tibia, when compared to the C-L or CNTRL group knees (Fig. 3). The PG loss also occurred in the pericellular regions, but not as strongly (Figs. 4 and 5). This result indicates that PGs may be bound more strongly to the PCM than the ECM, or chondrocytes have started to synthesize new PGs in response to the altered loading conditions or the ECM PG loss. However, in early and late OA human cartilage, the ratio of the PCM and surrounding ECM PG content stayed constant during OA progression (Korhonen et al., 2011). Based on this finding, the retention of the pericellular PGs after the PM as observed here could be a transient phenomenon.

The PG content in the PCM was also lower in the C-L group patellar cartilages compared to the CNTRL group samples (Fig. 4). Altered loading of the patella in the operated contralateral rabbit limb may produce this difference. However, we observed no differences in any other parameter between these two groups. As alterations in the contralateral joint have been previously reported at time periods longer than the one studied here (Mäkelä et al., 2014; Ojanen et al., 2018), one needs to be cautious when using contralateral limb as a normal control reference.

Consistent with a previous study (Colombo et al., 1983), the collagen network was not significantly affected at this early time point after the PM intervention (Supplemental Figs. 4 and 5). As lesions have been observed previously 1 to 2 weeks after PM on

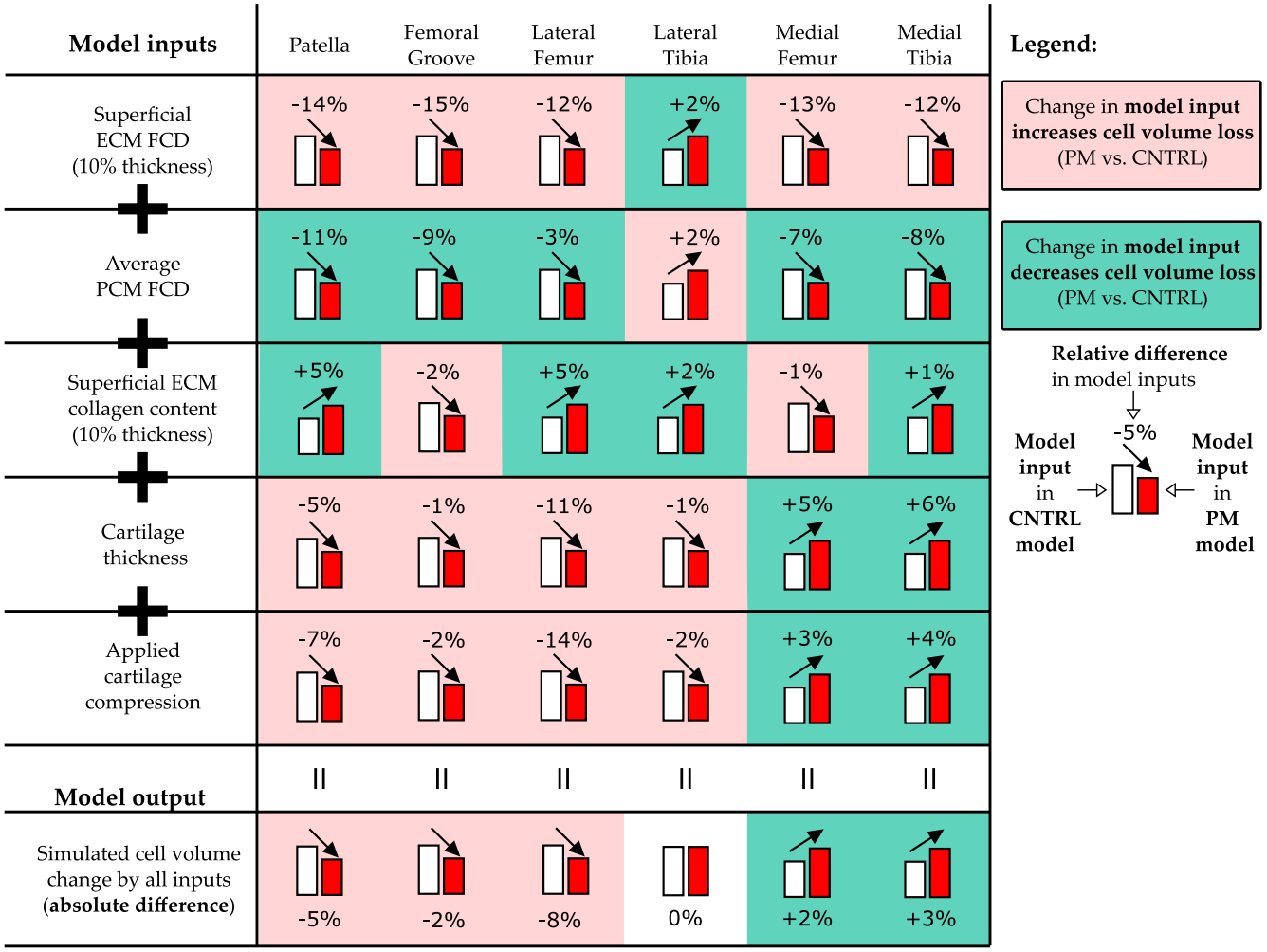

Fig. 8. Summary of all differences between the CNTRL and PM groups in the FE models for each knee joint location (separate column for each knee joint location). Each row corresponds to a single parameter in the FE model that was different between the CNTRL and the PM group, and the relative difference in parameter value between the PM model and CNTRL model is given as percentage. When we add up the effect of all the differences (conveyed by the +signs between the rows) for a given knee joint location, we end up in the cell volume change difference between the CNTRL and PM group models as given in the last row. This is conveyed with the rotated equal signs on top of the last row. The background color of each cell indicates what the effect of each single parameter difference on the cell volume change would be, if this was the sole difference between the CNTRL and PM models (so other parameters would be same between the models). A green background indicates that the given difference due to PM will cause decreased cell volume loss, whereas red background color indicates increased cell volume loss. (For interpretation of the references to color in this figure legend, the reader is referred to the web version of this article.)

both the femoral and tibial cartilages (Lindhorst et al., 2005), it is possible that the collagen network is disorganized in a ultrastructural fibril-level, for example, the fibril network interconnectivity could be reduced (Nickien et al., 2017). With the current methods, we only capture the collagen content and primary orientation of the collagen network; hence, this kind of changes could go unnoticed. Another possibility is that collagen damage follows the initial PG loss (Hunziker, 2002). One pathway for this sequence of events could arise from a reduced cartilage fluid pressurization due to the loss of FCD, predisposing the collagen matrix to higher strains than one would expect in normal cartilage and subsequent damage (Maroudas, 1976). This hypothesis is supported by the observation that cartilage softening has been suggested to precede collagen damage (Hosseini et al., 2013), and the fact that aggrecan is more prone to degradation than the cartilage collagen network (Roughley and Mort, 2014). However, it remains unknown if fluid pressurization of cartilage in the knee was indeed altered due to the amount of PG loss observed here, and future studies should investigate this.

5.3. Computational analysis of cell-tissue interactions

To explain site-specific volume responses of chondrocytes to indentation loading in our models, we summarized the differences observed between the CNTRL and PM group models, and studied how each parameter affects cell volume behavior (Fig. 8). The collagen content differences between groups were statistically non-significant; however, slight differences are present in the models, as collagen content is implemented according to the mean profiles (Supplemental Fig. 2). A smaller superficial collagen content would be related to an amplified loss in cell volume (Ronkainen et al., 2016). The final parameters that differed between the CNTRL and PM models were cartilage thickness and applied compression (Fig. 8). Thicker cartilage has a thicker superficial and middle zone, which leads to a reduced cell volume loss, according to the parametric investigation (Fig. 8). Surprisingly, at the experimental strains used here, higher absolute tissue compression reduced cell volume loss. This finding was explained by the higher in-plane cell elongations perpendicular to the compression axis, possibly due to the local collagen orientation and the increasing depth-wise PG content. Altogether, the ECM and PCM FCD losses, differences in cartilage structure and in absolute compression between the CNTRL and PM groups are in agreement with the altered cell volume changes at each location (Fig. 8).

5.4. Limitations

The limitations of this study are discussed briefly here and in more detail in the supplementary materials. First, the FE models have a simplified geometry and material properties compared to the reality. These simplifications warrant a degree of caution as the potential variability in input parameters could produce different modeling results relative to the experimental studies, especially when trying to investigate small chondrocyte volume changes (<10%). In addition, due to differences in cartilage biology and mechanics, relating the current findings to human tissue must be done with caution. Finally, the FE model does not account for biological events, such as inflammation, that could affect the mechanical results.

5.5. Conclusions

Loss of PG content was evident 3 days after the PM surgery in the cartilage superficial ECM and in the PCM surrounding cells. In contrast, there were no observable changes to the collagen network. As shown in the FE model results, increased cell volume losses following PM surgery (e.g., in the patellar samples) were associated with a loss of PGs in the cartilage ECM, whereas a loss of PGs in the PCM allowed for increased cell swelling and reduced cell volume losses (e.g., in the medial femoral samples). As such, reversing or preventing the PG loss may allow cells to maintain their normal physiological response to load, thereby slowing the progression of cartilage degeneration after PM surgery. In addition, cell volume changes were highly sensitive to collagen orientation, implying that it is important to incorporate realistic collagen network structure in cell-level FE models of articular cartilage.

6. Ethics statement on research of animals

All experiments were carried out according to the guidelines of the Canadian Council on Animal Care and were approved by the committee on Animal Ethics at the University of Calgary.

Author contributions

All authors were involved in (1) the conception and design of the study, and analysis and interpretation of data; (2) in drafting and revising the article critically for important intellectual content and (3) in final approval of the version to be submitted.

Acknowledgements

European Research Council under the European Union's Seventh Framework Programme (FP/2007-2013)/ERC Grant Agreement no. 281180; Academy of Finland (grant 286526); Sigrid Juselius Foundation; the Canada Research Chair Programme, the Killam Foundation; the Canadian Institutes of Health Research and the Finnish Cultural Foundation. In addition, the authors want to thank Aino Reunamo, M.Sc., University of Eastern Finland, for assistance in the DD measurements.

Role of funding sources

Funding sources were not involved in the study design, in the collection, analysis and interpretation of data; in the writing of the manuscript; or in the decision to submit the manuscript for publication.

Conflict of interest disclosure

Authors have nothing to disclose.

Appendix A. Supplementary material

Supplementary data to this article can be found online at https://doi.org/10.1016/j.jbiomech.2018.11.024.

References

Arunakul, M., Tochigi, Y., Goetz, J.E., Diestelmeier, B.W., Heiner, A.D., Rudert, J., Fredericks, D.C., Brown, T.D., McKinley, T.O., 2013. Replication of chronic abnormal cartilage loading by medial meniscus destabilization for modeling osteoarthritis in the rabbit knee in vivo. J. Orthop. Res. 31, 1555–1560. https://doi.org/10.1002/jor.22393.

Camacho, N.P., West, P., Torzilli, P.A., Mendelsohn, R., 2001. FTIR microscopic imaging of collagen and proteoglycan in bovine cartilage. Biopolymers 62, 1–8. https://doi.org/10.1002/1097-0282(2001) 62:1<1::AID-BIP10>3.0.CO;2-O.

Colombo, C., Butler, M., O'Byrne, E., Hickman, L., Swartzendruber, D., Selwyn, M., Steinetz, B., 1983. A new model of osteoarthritis in rabbits. I. Development of knee joint pathology following lateral meniscectomy and section of the fibular collateral and sesamoid ligaments. Arthritis Rheum. 26, 875–886.

de Vries, S.A.H., van Turnhout, M.C., Oomens, C.W.J., Erdemir, A., Ito, K., van Donkelaar, C.C., 2014. Deformation thresholds for chondrocyte death and the

protective effect of the pericellular matrix. Tissue Eng. Part A 20, 1870–1876. https://doi.org/10.1089/ten.tea.2013.0436.
Elder, S.H., Goldstein, S.A., Kimura, J.H., Soslowsky, L.J., Spengler, D.M., 2001. Chondrocyte differentiation is modulated by frequency and duration of cyclic compressive loading. Ann. Biomed. Eng. 29, 476–482. https://doi.org/10.1114/1.1376696.
Fick, J.M., Ronkainen, A., Herzog, W., Korhonen, R.K., 2015. Site-dependent biomechanical responses of chondrocytes in the rabbit knee joint. J. Biomech. 48, 4010–4019. https://doi.org/10.1016/j.jbiomech.2015.09.049.
Fick, J.M., Ronkainen, A.P., Madden, R., Sawatsky, A., Tiitu, V., Herzog, W., Korhonen, R.K., 2016. Early in situ changes in chondrocyte biomechanical responses due to a partial meniscectomy in the lateral compartment of the mature rabbit knee joint. J. Biomech. 49, 4057–4064. https://doi.org/10.1016/j.jbiomech.2016.10.039.
Florea, C., Tanska, P., Mononen, M.E., Qu, C., Lammi, M.J., Laasanen, M.S., Korhonen, R.K., 2016. A combined experimental atomic force microscopy-based nanoindentation and computational modeling approach to unravel the key contributors to the time-dependent mechanical behavior of single cells. Biomech. Model. Mechanobiol. 16, 1–15. https://doi.org/10.1007/s10237-016-0817-y.
Guilak, F., Alexopoulos, L.G., Haider, M.A., Ting-Beall, H.P., Setton, L.A., 2005. Zonal uniformity in mechanical properties of the chondrocyte pericellular matrix: micropipette aspiration of canine chondrons isolated by cartilage homogenization. Ann. Biomed. Eng. 33, 1312–1318. https://doi.org/10.1007/s10439-005-4479-7.
Guilak, F., Erickson, G.R., Ting-Beall, H.P., 2002. The effects of osmotic stress on the viscoelastic and physical properties of articular chondrocytes. Biophys. J. 82, 720–727. https://doi.org/10.1016/S0006-3495(02)75434-9.
Halloran, J.P., Sibole, S., Van Donkelaar, C.C., Van Turnhout, M.C., Oomens, C.W.J., Weiss, J.A., Guilak, F., Erdemir, A., 2012. Multiscale mechanics of articular cartilage: potentials and challenges of coupling musculoskeletal, joint, and microscale computational models. Ann. Biomed. Eng. 40, 2456–2474. https://doi.org/10.1007/s10439-012-0598-0.
Han, S.K., Ronkainen, A.P., Saarakkala, S., Rieppo, L., Herzog, W., Korhonen, R.K., 2017. Alterations in structural macromolecules and chondrocyte deformations in lapine retropatellar cartilage 9 weeks after anterior cruciate ligament transection. J. Orthop. Res. 1–9. https://doi.org/10.1002/jor.23650.
Hoch, D.H., Grodzinsky, A.J., Koob, T.J., Albert, M.L., Eyre, D.R., 1983. Early changes in material properties of rabbit articular cartilage after meniscectomy. J. Orthop. Res. 1, 4–12. https://doi.org/10.1002/jor.1100010102.
Hosseini, S.M., Veldink, M.B., Ito, K., van Donkelaar, C.C., 2013. Is collagen fiber damage the cause of early softening in articular cartilage? Osteoarth. Cartilage 21, 136–143. https://doi.org/10.1016/j.joca.2012.09.002.
Hunziker, E.B., 2002. Articular cartilage repair: basic science and clinical progress. A review of the current status and prospects. Osteoarth. Cartilage 10, 432–463. https://doi.org/10.1053/joca.2002.0801.
Julkunen, P., Kiviranta, P., Wilson, W., Jurvelin, J.S., Korhonen, R.K., 2007. Characterization of articular cartilage by combining microscopic analysis with a fibril-reinforced finite-element model. J. Biomech. 40, 1862–1870. https://doi.org/10.1016/j.jbiomech.2006.07.026.
Julkunen, P., Wilson, W., Isaksson, H., Jurvelin, J.S., Herzog, W., Korhonen, R.K., 2013. A review of the combination of experimental measurements and fibril-reinforced modeling for investigation of articular cartilage and chondrocyte response to loading. Comput. Math. Methods Med. 2013, 1–23. https://doi.org/10.1155/2013/326150.
Julkunen, P., Wilson, W., Jurvelin, J., Korhonen, R.K., 2009. Composition of the pericellular matrix modulates the deformation behaviour of chondrocytes in articular cartilage under static loading. Med. Biol. Eng. Comput. 47, 1281–1290. https://doi.org/10.1007/s11517-009-0547-8.
Király, K., Lapveteläinen, T., Arokoski, J., Törrönen, K., Módis, L., Kiviranta, I., Helminen, H.J., 1996. Application of selected cationic dyes for the semiquantitative estimation of glycosaminoglycans in histological sections of articular cartilage by microspectrophotometry. Histochem. J. 28, 577–590. https://doi.org/10.1007/BF02331378.
Kiviranta, I., Jurvelin, J., Säämänen, A.M., Helminen, H.J., 1985. Microspectrophotometric quantitation of glycosaminoglycans in articular cartilage sections stained with Safranin O. Histochemistry 82, 249–255. https://doi.org/10.1007/BF00501401.
Korhonen, R.K., Julkunen, P., Jurvelin, J.S., Saarakkala, S., 2011. Structural and compositional changes in peri- and extracellular matrix of osteoarthritic cartilage modulate chondrocyte morphology. Cell. Mol. Bioeng. 4, 484–494. https://doi.org/10.1007/s12195-011-0178-7.
Korhonen, R.K., Julkunen, P., Wilson, W., Herzog, W., 2008. Importance of collagen orientation and depth-dependent fixed charge densities of cartilage on mechanical behavior of chondrocytes. J. Biomech. Eng. 130. https://doi.org/10.1115/1.2898725. 021003–1–11.
Korhonen, R.K., Tanska, P., Kaartinen, S.M., Fick, J.M., Mononen, M.E., 2015. New concept to restore normal cell responses in osteoarthritic knee joint cartilage. Exerc. Sport Sci. Rev. 43, 143–152. https://doi.org/10.1249/JES.0000000000000051.
Lindhorst, E., Wachsmuth, L., Kimmig, N., Raiss, R., Aigner, T., Atley, L., Eyre, D., 2005. Increase in degraded collagen type II in synovial fluid early in the rabbit meniscectomy model of osteoarthritis. Osteoarth Cartilage 13, 139–145. https://doi.org/10.1016/j.joca.2004.10.017.
Mansour, J.M., Wentorf, F.a., Degoede, K.M., 1998. In vivo kinematics of the rabbit knee in unstable models of osteoarthrosis. Ann. Biomed. Eng. 26, 353–360. 10.1114/1.133.
Maroudas, A.I., 1976. Balance between swelling pressure and collagen tension in normal and degenerate cartilage. Nature 260, 808–809. https://doi.org/10.1038/260808a0.
Mäkelä, J.T.A., Korhonen, R.K., 2016. Highly nonlinear stress-relaxation response of articular cartilage in indentation: importance of collagen nonlinearity. J. Biomech. 49, 1734–1741. https://doi.org/10.1016/j.jbiomech.2016.04.002.
Mäkelä, J.T.A., Rezaeian, Z.S., Mikkonen, S., Madden, R., Han, S.K., Jurvelin, J.S., Herzog, W., Korhonen, R.K., 2014. Site-dependent changes in structure and function of lapine articular cartilage 4 weeks after anterior cruciate ligament transection. Osteoarth. Cartilage 22, 869–878. https://doi.org/10.1016/j.joca.2014.04.010.
Nickien, M., Thambyah, A., Broom, N.D., 2017. How a decreased fibrillar interconnectivity influences stiffness and swelling properties during early cartilage degeneration. J. Mech. Behav. Biomed. Mater. 75, 390–398. https://doi.org/10.1016/j.jmbbm.2017.07.042.
Ojanen, S.P., Finnilä, M.A.J., Reunamo, A.E., Ronkainen, A.P., Mikkonen, S., Herzog, W., Saarakkala, S., Korhonen, R.K., 2018. Site-specific glycosaminoglycan content is better maintained in the pericellular matrix than the extracellular matrix in early post-traumatic osteoarthritis. PLoS One 13, 1–19. https://doi.org/10.1371/journal.pone.0196203.
Papalia, R., Del Buono, A., Osti, L., Denaro, V., Maffulli, N., 2011. Meniscectomy as a risk factor for knee osteoarthritis: a systematic review. Br. Med. Bull. 99, 89–106. https://doi.org/10.1093/bmb/ldq043.
Potter, K., Kidder, L.H., Levin, I.W., Lewis, E.N., Spencer, R.G., 2001. Imaging of collagen and proteoglycan in cartilage sections using Fourier transform infrared spectral imaging. Arthritis Rheum. 44, 846–855. https://doi.org/10.1002/1529-0131(200104)44:4<846::AID-ANR141>3.0.CO;2-E.
Rieppo, J., Hallikainen, J., Jurvelin, J.S., Kiviranta, I., Helminen, H.J., Hyttinen, M.M., 2008. Practical considerations in the use of polarized light microscopy in the analysis of the collagen network in articular cartilage. Microsc. Res. Tech. 71, 279–287. https://doi.org/10.1002/jemt.20551.
Ronkainen, A.P., Fick, J.M., Herzog, W., Korhonen, R.K., 2016. Site-specific cell-tissue interactions in rabbit knee joint articular cartilage. J. Biomech. 49, 2882–2890. https://doi.org/10.1016/j.jbiomech.2016.06.033.
Roughley, P.J., Mort, J.S., 2014. The role of aggrecan in normal and osteoarthritic cartilage. J. Exp. Orthop. 1, 8. https://doi.org/10.1186/s40634-014-0008-7.
Sharma, L., 2016. Osteoarthritis year in review 2015: clinical. Osteoarth. Cartilage 24, 36–48. https://doi.org/10.1016/j.joca.2015.07.026.
Sokoloff, L., 1990. Animal models of osteoarthritis. J. Rheumatol. 17, 5–6. https://doi.org/10.2174/157339708785133523.
Tanska, P., Turunen, S.M., Han, S.K., Julkunen, P., Herzog, W., Korhonen, R.K., 2013. Superficial collagen fibril modulus and pericellular fixed charge density modulate chondrocyte volumetric behaviour in early osteoarthritis. Comput. Math. Methods Med. 2013, 17–21. https://doi.org/10.1155/2013/164146.
Turunen, S.M., Han, S.K., Herzog, W., Korhonen, R.K., 2013. Cell deformation behavior in mechanically loaded rabbit articular cartilage 4 weeks after anterior cruciate ligament transection. Osteoarth. Cartilage 21, 505–513. https://doi.org/10.1016/j.joca.2012.12.001.
Wilson, W., 2005. A comparison between mechano-electrochemical and biphasic swelling theories for soft hydrated tissues. J. Biomech. Eng. 127, 158–165. https://doi.org/10.1115/1.1835361.
Wilson, W., Huyghe, J.M., van Donkelaar, C.C., 2006. A composition-based cartilage model for the assessment of compositional changes during cartilage damage and adaptation. Osteoarth. Cartilage 14, 554–560. https://doi.org/10.1016/j.joca.2005.12.006.
Wilson, W., van Donkelaar, C.C., van Rietbergen, B., Huiskes, R., 2005. A fibril-reinforced poroviscoelastic swelling model for articular cartilage. J. Biomech. 38, 1195–1204. https://doi.org/10.1016/j.jbiomech.2004.07.003.
Wilson, W., van Donkelaar, C.C., van Rietbergen, B., Ito, K., Huiskes, R., 2004. Stresses in the local collagen network of articular cartilage: a poroviscoelastic fibril-reinforced finite element study. J. Biomech. 37, 357–366. https://doi.org/10.1016/S0021-9290(03)00267-7.
Wilusz, R.E., Sanchez-Adams, J., Guilak, F., 2014. The structure and function of the pericellular matrix of articular cartilage. Matrix Biol. 39, 25–32. https://doi.org/10.1016/j.matbio.2014.08.009.